



1 **Frequent haze events associated with transport and stagnation over**
2 **the corridor between North China Plain and Yangtze River Delta**

3 Feifan Yan¹, Hang Su², Yafang Cheng², Rujin Huang³, Hong Liao⁴, Ting Yang⁵,
4 Yuanyuan Zhu⁶, Shaoqing Zhang⁷, Lifang Sheng⁸, Wenbing Kou¹, Xinran Zeng⁹,
5 Shengnan Xiang¹, Xiaohong Yao¹, Huiwang Gao¹, Yang Gao^{1*}

6 ¹Frontiers Science Center for Deep Ocean Multispheres and Earth System (FDOMES) and Key
7 Laboratory of Marine Environmental Science and Ecology, Ministry of Education, Ocean
8 University of China, and Laoshan Laboratory, Qingdao, 266100, China

9 ²Max Planck Institute for Chemistry, Multiphase Chemistry Department, Mainz D-55128, Germany

10 ³State Key Laboratory of Loess and Quaternary Geology (SKLLQG), Center for Excellence in
11 Quaternary Science and Global Change, Institute of Earth Environment, Chinese Academy of
12 Sciences, Xi'an 710061, China

13 ⁴Jiangsu Key Laboratory of Atmospheric Environment Monitoring and Pollution Control, Jiangsu
14 Engineering Technology Research Center of Environmental Cleaning Materials, Collaborative
15 Innovation Center of Atmospheric Environment and Equipment Technology, School of
16 Environmental Science and Engineering, Nanjing University of Information Science &
17 Technology, Nanjing 210044, China

18 ⁵State Key Laboratory of Atmospheric Boundary Layer Physics and Atmospheric Chemistry,
19 Institute of Atmospheric Physics, Chinese Academy of Sciences, Beijing, 100029, China

20 ⁶China National Environmental Monitoring Centre, Beijing 100012, China

21 ⁷Frontiers Science Center for Deep Ocean Multispheres and Earth System, and Key Laboratory of
22 Physical Oceanography, Ministry of Education, the College of Oceanic and Atmospheric Sciences,
23 Ocean University of China, and Laoshan Laboratory, Qingdao, 266100, China

24 ⁸College of Oceanic and Atmospheric Sciences, Ocean University of China, Qingdao, 266100,
25 China

26 ⁹Zhejiang Institute of Meteorological Sciences, Hangzhou, 310008, China

27

28

*Correspondence to: yanggao@ouc.edu.cn

29

30

31



32

Abstract

33 $PM_{2.5}$ pollution is a major air quality issue deteriorating human health, and
34 numerous studies focus on $PM_{2.5}$ pollution in major regions such as North China Plain
35 (NCP) and Yangtze River Delta (YRD). However, the characteristics of $PM_{2.5}$
36 concentrations and the associated formation mechanism in the transport corridor
37 (referred to as SWLY) between NCP and YRD are largely ignored. Based on
38 observational data, we find the number of $PM_{2.5}$ pollution events in SWLY is
39 comparable to that in NCP, far exceeding those in YRD, indicative of the severity of air
40 pollution over this area. Utilizing a regional climate and air quality model, we isolate
41 the effect of seesaw transport events, e.g., transport between NCP and YRD, as well as
42 the atmospheric stagnation on the accumulation of $PM_{2.5}$ over SWLY. Specifically,
43 seesaw events and stagnation, comparable to each other, collectively account for an
44 average of 67% pollution days with $PM_{2.5}$ exceeding $75 \mu\text{g}/\text{m}^3$, and this fraction (85%)
45 is even larger for severe haze events with $PM_{2.5}$ exceeding $150 \mu\text{g}/\text{m}^3$. Furthermore, the
46 connection between seesaw transport and large-scale circulation is examined. The
47 trans-regional transport of pollutants from NCP to YRD (YRD to NCP) is likely
48 stimulated by positive (negative) to negative (positive) geopotential height anomaly at
49 500 hPa located in northern China. The health effect due to short-term $PM_{2.5}$ exposure
50 induced by the trans-regional transport and stagnation is investigated, yielding a total
51 of 8,634 (95% CI: 6,023-11,223) and 9,496 (95% CI: 6,552-12,413) premature deaths
52 respectively in SWLY during winter 2014-2019, as high as 9% of the total premature
53 deaths in China although the area coverage of SWLY is within 1%. While atmospheric
54 stagnation is in general projected to occur more frequently under a warming climate,
55 this study indicates the importance of regional emission control to alleviate $PM_{2.5}$
56 pollution from seesaw transport and stagnation.

57

58

59

60



61 **1 Introduction**

62 With the rapid development of the economy, particulate matter with diameters less
63 than 2.5 μm ($\text{PM}_{2.5}$) has become a major issue deteriorating air quality in China and
64 threatening human health, e.g., causing serious respiratory, cardiovascular diseases and
65 even premature death (Donaldson et al., 1998; Pui et al., 2014; Xing et al., 2016). Strict
66 emission control strategies have been carried out since the severe haze pollution events
67 in 2013, leading to a generally decreasing trend of annual mean $\text{PM}_{2.5}$ concentrations
68 (Zhang et al., 2019b). Nevertheless, besides emissions, unfavorable meteorological
69 conditions, such as atmospheric stagnation (Gao et al., 2020; Wang et al., 2022) and
70 trans-regional transport of air pollutants (Huang et al., 2020; Kang et al., 2021; Ma et
71 al., 2017), remain to stimulate the accumulation of local $\text{PM}_{2.5}$, conducive to
72 exceedance of Chinese Ambient Air Quality Standards.

73 In China, severe $\text{PM}_{2.5}$ pollution in eastern China has received a lot of attention,
74 especially in North China Plain (NCP) (Wang et al., 2014; Zhang et al., 2015) and the
75 Yangtze River Delta (YRD) (Jia et al., 2022; Li et al., 2019a). Several studies pointed
76 out that air pollutants can be transported between NCP and YRD (He et al., 2018; Huang
77 et al., 2020; Kang et al., 2019; Zhang et al., 2021a). For instance, by applying the source
78 apportionment method, Kang et al. (2019) found that the transport due to cold frontal
79 passage from NCP contributed to 29% of the severe $\text{PM}_{2.5}$ pollution with $\text{PM}_{2.5}$
80 concentrations as high as 300 $\mu\text{g m}^{-3}$ during 21–26 January 2015 in YRD. Similarly,
81 Huang et al. (2020) found that the air pollutant from YRD could transport to NCP,
82 lowering the planetary boundary layer height (PBLH) through aerosol direct radiative
83 effect and aggravate the accumulation of $\text{PM}_{2.5}$ concentrations therein, which can then
84 be transported back to YRD by cold fronts. In fact, the region located in the connecting
85 belt of these two areas, particularly at the junction of four provinces (Jiangsu, Anhui,
86 Shandong, Henan) referred to as SWLY, experiences heavy $\text{PM}_{2.5}$ pollution in China
87 (Wu et al., 2018; Xie et al., 2016). Moreover, high $\text{PM}_{2.5}$ concentrations pose a
88 remarkable health risk due to the dense population in SWLY (Li et al., 2019b; Yang et
89 al., 2018). Nevertheless, there are very limited studies investigating the transport effects



90 on $PM_{2.5}$ concentrations in SWLY.

91 Besides the transport, atmospheric stagnation plays an essential role in magnifying
92 local air pollution in China. Previous studies indicated that atmospheric stagnation
93 exhibited a high spatial correlation with $PM_{2.5}$ pollution over eastern China (Wang et
94 al., 2022) and favored the accumulation in $PM_{2.5}$ concentrations (Gao et al., 2020; Wang
95 et al., 2018b). For instance, Wang et al. (2022) found that more than two thirds of
96 stagnant days could lead to high $PM_{2.5}$ concentrations exceeding the 90th percentile in
97 NCP during 2013-2018. During 1985-2014, the most evident increasing trend of
98 atmospheric stagnation frequency was found in the eastern flank of China, including
99 the SWLY region (Huang et al., 2017), and how these weather conditions induce $PM_{2.5}$
100 pollution over there remains unclear.

101 $PM_{2.5}$ exerts substantial health effects, among which long-term exposure effect has
102 been widely acknowledged (REF), and recent studies indicated striking health burdens
103 resulting from short-term exposure to $PM_{2.5}$ as well (Jiang et al., 2020; Li et al., 2019b;
104 Liu et al., 2021). For example, Li et al. (2019b) found 169,862 additional deaths
105 attributed to short-term $PM_{2.5}$ exposure in China in 2015, with the highest death rate of
106 14.63 (95%CI: 8.50-20.69) per 100,000 people in the eastern China. Liu et al. (2021)
107 found that Shandong, Jiangsu, Hebei, and Henan experienced the highest health cost
108 (medical cost, productivity loss, etc.) in China attributable to short-term $PM_{2.5}$ pollution
109 during 2013-2018. Therefore, it is of great importance to investigate the health burdens
110 associated with short-term exposure to $PM_{2.5}$ concentrations, as well as the
111 contributions resulting from different meteorological conditions, e.g., trans-regional
112 transport and stagnant weather in SWLY.

113 To this end, we conduct the numerical simulations with Weather Research and
114 Forecasting (WRF) and Community Multiscale Air Quality (CMAQ) from 2014 to
115 2019, aiming to isolate the effects of transport (section 3.2) and atmospheric stagnation
116 (section 3.3) on $PM_{2.5}$ in SWLY. At the end, the health impact of $PM_{2.5}$ caused by trans-
117 regional transport and stagnation is quantified.

118



119 **2 Model configuration and methods**

120 **2.1 Model configuration**

121 This study applies WRF version 4.1.1 and CMAQ version 5.3.1 to simulate the
122 meteorological and air quality conditions from 2014 to 2019. The simulation domain is
123 shown in Fig. S1, and the spatial resolution is 36 km × 36 km. There are 34 vertical
124 layers from surface to 50 hPa with denser layers within the planetary boundary layer
125 (PBL) to better reproduce the air pollutant concentrations within the layer (Appel et al.,
126 2007; Wang et al., 2011). The physics schemes in WRF are shown in Table S1,
127 consistent with the previous study (Zeng et al., 2022). The NCEP Climate Forecast
128 System Reanalysis (CFRS) version 2 (Saha et al., 2014), with horizontal resolutions of
129 0.5° × 0.5°, provides the initial and boundary conditions for WRF simulations. The gas
130 chemical mechanism of Carbon-Bond version 6 (CB6) (Luecken et al., 2019) and the
131 aerosol module of AERO7 are used (Appel et al., 2021; Pye et al., 2017). The chemical
132 initial and boundary conditions of CMAQ are downscaled from the Model for Ozone
133 and Related chemical Tracers, version 4 (MOZART-4) (Emmons et al., 2010), the same
134 method as applied in Ma et al. (2019).

135 In this study, anthropogenic emissions inventory in the year of 2016 is derived
136 from the Multi-resolution Emission Inventory for China version 1.2 (MEIC v1.2;
137 <http://www.meicmodel.org> (Li et al., 2017; Zheng et al., 2018)), which mainly includes
138 emissions from agriculture, resident, transportation, industry and power plants. The
139 ship emissions are from Shipping emission inventory model (SEIM) (Liu et al., 2016;
140 Liu et al., 2019b). The biomass burning emission inventory from 2014-2019 is based
141 on Global Emission Database version 4.1 (GFEDv4.1; (Giglio et al., 2013; Van der Werf
142 et al., 2017)). The hourly biogenic emissions are generated by Model of Emission of
143 Gases and Aerosol from Nature (MEGAN) (Guenther et al., 2012). For the evaluation
144 of model simulations, the meteorological observation data is available at the National
145 Climatic Data Center (NCDC, [https://www.ncdc.noaa.gov/data-access/quick-
146 links#dsi-3505](https://www.ncdc.noaa.gov/data-access/quick-links#dsi-3505); last access: December 8, 2021), including air temperature at 2 m, wind
147 speed and direction at 10 m. The observational hourly PM_{2.5} data are taken from the



148 China National Environmental Monitoring Centre (<http://www.pm25.in>, last access:
149 September 23, 2021). In this study, the three months (January, February, and December)
150 of each year, referred to as the season of winter, is focused considering it is the major
151 haze period.

152 **2.2 Short-term exposure premature death to PM_{2.5}**

153 In order to quantify the health effect attributable to exposure to PM_{2.5}, we calculate
154 all-cause premature deaths associated with the short-term exposure to PM_{2.5} during
155 2014-2019. The formula is used as shown below:

$$156 \quad RR_{i,j} = \exp[\beta \times \max(C_{i,j} - C_0, 0)]$$

157 $RR_{i,j}$ represents the relative risk for deaths from all-cause, where i and j represent
158 the day and grid, respectively. $C_{i,j}$ is the daily average concentration of PM_{2.5}. For the
159 days with mean PM_{2.5} greater than or equal to $75 \mu\text{g m}^{-3}$, C_0 equals to $75 \mu\text{g m}^{-3}$, and
160 the exposure-response coefficient β is set to be 1.22% (95% CI: 0.82–1.63%) per 10
161 $\mu\text{g m}^{-3}$ increase of PM_{2.5} (Sun et al., 2022). For all the other days which are considered
162 relatively clean, C_0 equals to zero, β is set to be 0.41% (95% CI: 0.32–0.50%) per 10
163 $\mu\text{g m}^{-3}$ increase of PM_{2.5} (Liu et al., 2019a). The age structure is not considered in this
164 formula because of little significant differences in mortality among age subgroups (Sun
165 et al., 2022).

$$166 \quad \text{Death}_{i,j} = Y_{i,j} \times P_j \times (1 - 1/RR_{i,j})$$

167 $\text{Death}_{i,j}$ represents the number of premature deaths at a specific grid on a day;
168 $Y_{i,j}$ is the daily baseline mortality rate, which is obtained from the Global Burden of
169 Disease (GBD) 2019 data (<https://vizhub.healthdata.org/gbd-results/>; (Berman et al.,
170 2020)). P_j represents the number of populations.

171 **2.3 Definition of seesaw events and air stagnation**

172 In this study, we focus on two meteorological scenarios during wintertime in 2014-
173 2019: seesaw events and air stagnation. The seesaw events are diagnosed as follows:
174 over a three-day period, the mean PM_{2.5} concentration over NCP (YRD) decreases by
175 more than a certain threshold whereas it increases continuously during the period over



176 YRD (NCP), leading to two type of seesaw events. In this study, we select a threshold
177 of 40%, which identified a total of 168 days with the seesaw pattern. Additionally, we
178 test several other thresholds (e.g., 30%, 35%, 45%, 50%), which resulted in comparable
179 numbers of seesaw pattern days: 182, 176, 162, 154, respectively. Regarding air
180 stagnation, we adopted the criteria proposed by Gao et al. (2020). A stagnant day is
181 defined as a day where the daily mean wind speed at 10 m is less than 3.2 m/s, the daily
182 total precipitation is less than 1 mm and the planetary boundary layer height is less than
183 520 m.

184 Please note that there is an overlap between stagnant and seesaw events. Among
185 the seesaw events, 35% are concomitant with stagnant conditions, indicating that the
186 seesaw events together with stagnant weather conditions are more conducive to high
187 PM_{2.5} pollution. As a result, when discussing the seesaw pattern, the concomitant
188 stagnant days are included.

189

190 **3 Results and discussions**

191 **3.1 Model validation**

192 To evaluate the capability of model in reproducing the observations, we first
193 compared the meteorological parameters, including daily air temperature at 2 m (T₂),
194 specific humidity at 2 m (Q₂), wind speed at 10 m (WS₁₀) and wind direction at 10 m
195 (WD₁₀), simulated by WRF (Table S2) against the observations of the NCDC over
196 NCP, YRD, and SWLY. The statistical metrics, including mean bias, gross error, and
197 root-mean-square error (RMSE), are mostly within the benchmarks (Emery and Tai,
198 2001), despite the slightly higher bias for wind direction which is likely attributable to
199 wind directions close to 0° or 360° (Zhang et al., 2019a). Moreover, daily mean
200 simulated PM_{2.5} is compared to observations during 2014-2019 over the three regions
201 of NCP, YRD, and SWLY (Fig. S2). Overall, the mean fractional bias (MFB) and mean
202 fractional error percent (MFE) are within the benchmarks (MFB ≤ ±50%, MFE ≤ 75%,
203 US EPA (2007)), warranting a high confidence of interpreting the simulated results.

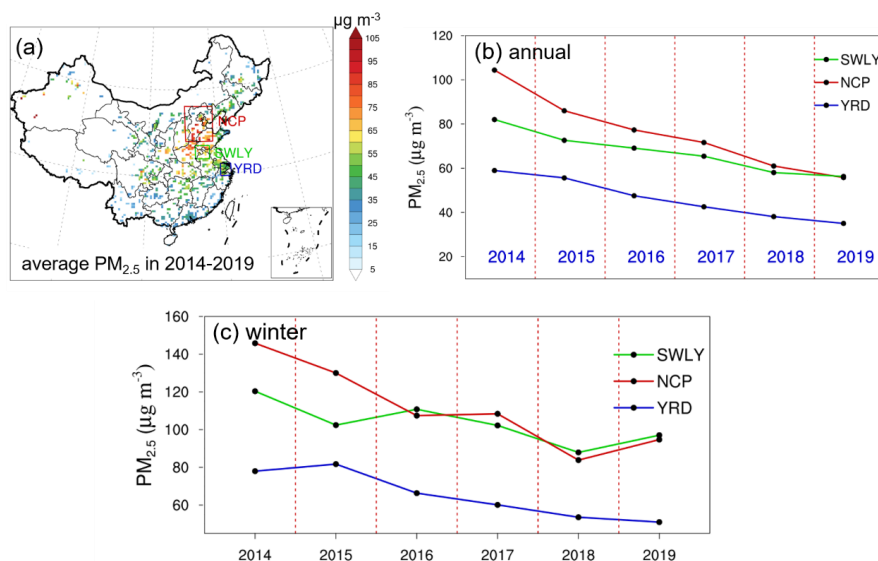
204



205 **3.2 Observational evidence of high PM_{2.5} concentrations in SWLY**

206 Figure 1a shows the spatial distribution of observed mean PM_{2.5} concentrations
 207 from 2014 to 2019. The high values of PM_{2.5} predominantly concentrate in eastern
 208 China due to dense populations and anthropogenic emissions (Gao et al., 2022).
 209 Zooming into the SWLY, NCP and YRD, the annual mean PM_{2.5} in these three regions
 210 gradually decreases, primarily attributable to strict clean air policies and reductions in
 211 anthropogenic emissions (Zhang et al., 2019b). Among the three regions, the average
 212 PM_{2.5} concentration is highest in NCP (76.0 μg m⁻³), followed closely by SWLY with
 213 PM_{2.5} concentrations of 67.2 μg m⁻³, much higher than that over YRD (46.3 μg m⁻³).
 214 Furthermore, as shown in Fig. 1b, despite the adjacency of the SWLY to NCP, the
 215 decreasing trend is more pronounced in NCP (9.3 μg m⁻³ a⁻¹), followed by YRD (5.1 μg
 216 m⁻³ a⁻¹), and SWLY (5.0 μg m⁻³ a⁻¹). When focusing specifically on the winter season,
 217 as shown in Fig. 1c, PM_{2.5} concentrations in NCP and SWLY are almost comparable
 218 from 2016 to 2019 and much higher than in YRD, indicating a more severe haze
 219 pollution situation in winter in SWLY compared to YRD. Note that the line separation
 220 between NCP and SWLY in winter of 2014 and 2015 will be discussed in the subsequent
 221 paragraph.

222



223



224 Figure 1. a: Spatial distribution of six-year annual mean $PM_{2.5}$. b,c: Time series of
225 annual (b) and winter (c) mean $PM_{2.5}$ concentrations over SWLY, NCP, and YRD
226 regions.

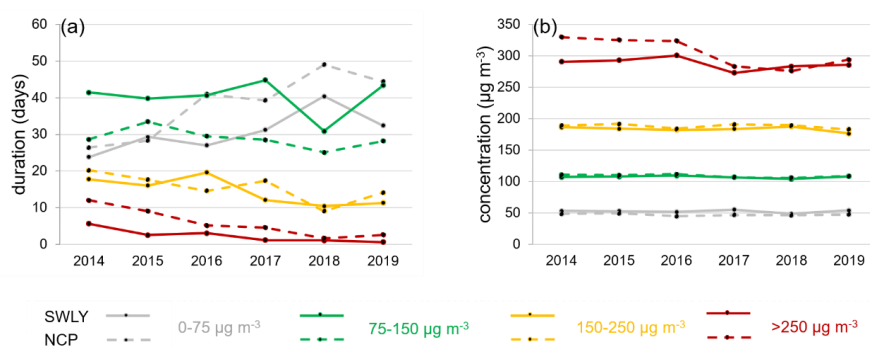
227

228 According to the Air Quality Index (HJ 633-2012; (MEEPRC, 2012)), a pollution
229 day is defined as a day with mean $PM_{2.5}$ concentration exceeding $75 \mu g m^{-3}$, which can
230 be further divided into moderate pollution ($75-150 \mu g m^{-3}$), heavy pollution ($150-250$
231 $\mu g m^{-3}$) and extreme pollution (greater than $250 \mu g m^{-3}$). To better measure the severity
232 of pollution, a metric of duration is induced, which is calculated as the regional mean
233 value of total number of pollution days in winter. The number of pollution days in one
234 event is considered as persistence, and we have also calculated the mean persistence of
235 all events. Figure 2 shows the duration, as well as mean regional $PM_{2.5}$ concentrations
236 over SWLY and NCP during these pollution days, for these three categories
237 abovementioned. Here, some discussion is needed to show why we introduce these
238 parameters, and which kind of information it could bring us beyond a simple $PM_{2.5}$
239 concentration.

240 During wintertime in 2014-2019, the total annual number of pollution days reaches
241 on average of 57.1 and 50.3 in SWLY and NCP, respectively (Fig. 2a). By classifying
242 pollution days into different categories, the results depicted in Fig. 2b indicate that the
243 extreme pollution events, characterized by daily mean $PM_{2.5}$ concentrations exceeding
244 $250 \mu g m^{-3}$, dominate the interannual variability of winter $PM_{2.5}$ in both SWLY and
245 NCP (Fig. 1c). Similarly, as shown in Fig. S4, in 2014 and 2015, the cumulative
246 distribution function curves of daily observational $PM_{2.5}$ in NCP are obviously on the
247 right of that in SWLY, indicating higher $PM_{2.5}$ concentrations over NCP. Since 2016,
248 the cumulative distribution function curves over SWLY are on the right of that in NCP
249 when $PM_{2.5}$ concentration is below $100-150 \mu g m^{-3}$, which reverses when $PM_{2.5}$
250 concentration becomes higher, yielding an overall comparable $PM_{2.5}$ concentration
251 between NCP and SWLY. While both SWLY and NCP experience comparably frequent
252 $PM_{2.5}$ pollution events, higher than that over YRD (Fig. S5a), the higher total number



253 of PM_{2.5} pollution days in SWLY indicates that the meteorological features in SWLY
 254 may govern the severe pollution over there, considering that the mean precursor
 255 emissions (such as NO_x and SO₂) in SWLY are only 68% and 52% of those in the NCP
 256 (Fig. S6).
 257



258
 259 Figure 2. The regional mean number of days (duration) (a) and concentrations (b) of
 260 observational PM_{2.5} for the four categories (I: 0-75 µg m⁻³, II: 75-150 µg m⁻³, III: 150-
 261 250 µg m⁻³ and IV: greater than 250 µg m⁻³) over SWLY (solid lines) and NCP (dotted
 262 lines) in winter from 2014 to 2019.

263

264 3.3 The seesaw effect between NCP and YRD on PM_{2.5} in SWLY

265 Considering that SWLY is located in the corridor between NCP and YRD, the
 266 transport from the polluted area such as NCP and YRD could play key roles affecting
 267 air quality in SWLY. To diagnose the effect, two types of seesaw events are defined in
 268 this study. Type I seesaw events are characterized by a decrease (40% threshold) in
 269 PM_{2.5} concentration over NCP and an increase over YRD, while Type II seesaw events
 270 show the opposite pattern.

271 The temporal evolution of mean composited PM_{2.5} concentrations during winter
 272 2014-2019 in SWLY, NCP and YRD for Type I and II seesaw events are shown in Fig.
 273 3a-b. For Type I events (Fig. 3a), there is a total of 24 events lasting 75 days, with a
 274 persistence on average of 3 days. On day 1, the PM_{2.5} concentrations are highest over
 275 NCP (144.5 µg m⁻³), followed by SWLY (103.9 µg m⁻³) and YRD (32.1 µg m⁻³),

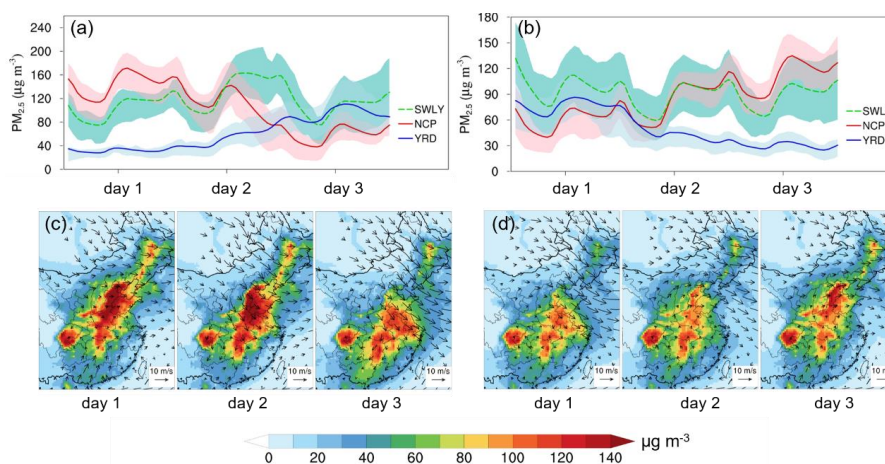


276 respectively. On day 2, along with a sharp decrease in $PM_{2.5}$ concentration in NCP
277 ($112.9 \mu\text{g m}^{-3}$), the $PM_{2.5}$ in SWLY rapidly increases by 31% ($135.2 \mu\text{g m}^{-3}$). Finally,
278 on the third day, when $PM_{2.5}$ pollution is cleared out in NCP ($59.0 \mu\text{g m}^{-3}$), $PM_{2.5}$
279 concentrations in SWLY remains to be as high as $108.7 \mu\text{g m}^{-3}$ and it increases to 94.3
280 $\mu\text{g m}^{-3}$ in YRD. Fig. 3c further denotes wind vectors at 850 hPa which supports the
281 movement of surface $PM_{2.5}$ concentration. On day 1, the weak wind over North China
282 favors the accumulation of $PM_{2.5}$ in NCP, and the particulate matters propagate
283 southeastward driven by the enhanced northwesterly wind, resulting in high $PM_{2.5}$
284 concentrations in SWLY and YRD on day 2 and 3. Previous studies have pointed out
285 the trans-boundary effect from NCP to YRD contributed to almost one third of total
286 $PM_{2.5}$ in YRD during the periods such as January 21-26, 2015 (Kang et al., 2019) and
287 November 2-3, 2017 (Kang et al., 2021), respectively.

288

289 Similarly, in Type II events (Fig. 3b) during which $PM_{2.5}$ is transported from YRD
290 toward northwest direction, there is a total of 106 days with 32 events. Compared to
291 day 1, $PM_{2.5}$ concentrations in day 3 over YRD decreases rapidly by 63%, while it
292 increases by 82% over NCP ($111.7 \mu\text{g m}^{-3}$). Meanwhile, SWLY maintains a stable
293 pollutant status, with $PM_{2.5}$ concentrations of 59.4 - $131.9 \mu\text{g m}^{-3}$. The spatiotemporal
294 evolution of surface $PM_{2.5}$ concentrations and wind vector at 850 hPa during this event
295 is displayed in Fig. 3d. Unlike Type I (Fig. 3c), on day 1, strong northwesterly wind in
296 northern China is concomitant with low $PM_{2.5}$ concentrations over NCP, while the $PM_{2.5}$
297 in southern China such as YRD and the adjacent areas are relatively high. In the
298 following two days, the northwesterly wind retreat further north, and weak southerly
299 wind dominates the majority of North China, stimulating the accumulation of $PM_{2.5}$ in
300 SWLY and NCP. Comparably, focusing an episodic events during October 29 to
301 November 6, 2015 over NCP, Zhang et al. (2021b) found that transport from the south
302 could account for up to 70% of $PM_{2.5}$ concentrations over this area.

303



304

305 Figure 3. First row: Time series of mean $PM_{2.5}$ concentrations in the SWLY (green
 306 dashed line), NCP (red solid line) and YRD (blue solid line), with shading indicative of
 307 the range of 25th -75th percentile, during 2014-2019 for type I (a) and type II (b). Second
 308 row: The spatial distribution shows the surface average $PM_{2.5}$ concentrations during
 309 three days in type I (c) and type II (d), respectively, with black arrows representing the
 310 wind vectors at 850 hPa.

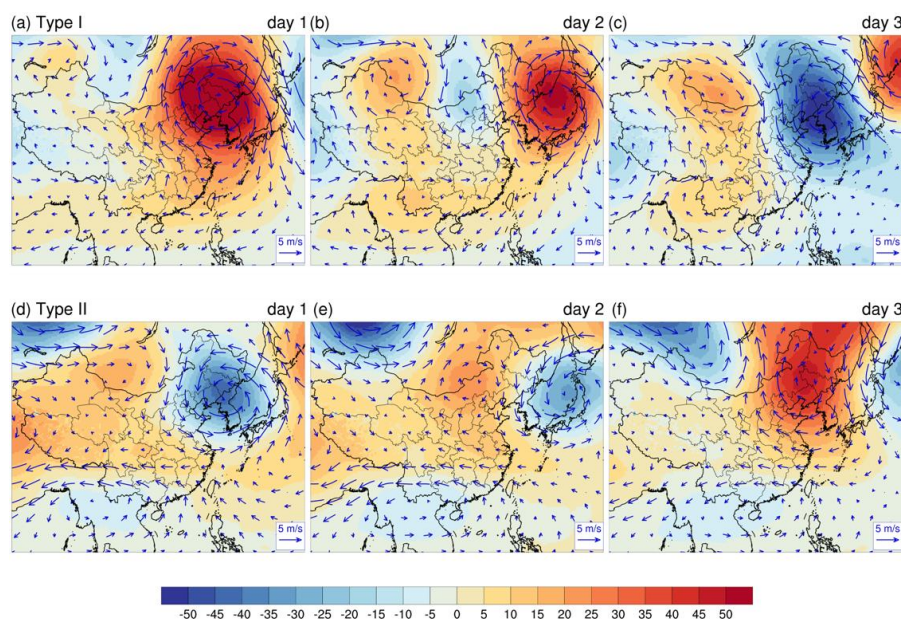
311

312 There is a tight relationship between surface $PM_{2.5}$ concentration and upper-level
 313 large scale circulations (e.g., 500 hPa) in eastern China (Hua and Wu, 2022; Zhang et
 314 al., 2022). To this end, we composite the anomalous 500 hPa geopotential height and
 315 wind vector during Type I and II events. As shown in Fig. 4a, for Type I, NCP is located
 316 westward of the intense anticyclonic anomalies center, conducive to accumulation of
 317 $PM_{2.5}$ concentrations therein through inducing relatively stagnant weather conditions
 318 (Wang et al., 2020; Zhong et al., 2019). Based on observations during 2009-2020 as
 319 mentioned in Hua and Wu (2022), the negative-positive height anomalies could be
 320 regarded as a reliable signal for wintertime haze occurrence in Beijing. On day 2 and 3,
 321 the high-pressure system center retreat eastward, and a triple feature emerges, with
 322 positive-negative-positive in northern of China from west to east, and the middle low-
 323 pressure system favors the air transport from North China Plain, eventually form the
 324 high $PM_{2.5}$ in SWLY and YRD. In contrast, the spatial evolution of pressure system



325 behaves oppositely for Type II events (Fig. 4b). The North China is controlled by a low-
 326 pressure system on the day 1, supporting the low $PM_{2.5}$ over there and relatively high
 327 $PM_{2.5}$ over YRD and southern China. Along with the movement of air flow, a high
 328 pressure system kicks in and take over, facilitating transport of moist and warm airflow
 329 and subsequently secondary formation of $PM_{2.5}$ in northern China (Zhang et al., 2022;
 330 Zhang et al., 2021b).

331



332

333 Figure 4. The composite anomalies of geopotential height (units: gpm) and wind
 334 vector at 500 hPa for three days for Type I and Type II, with the anomaly relative to the
 335 winter average in 2014-2019.

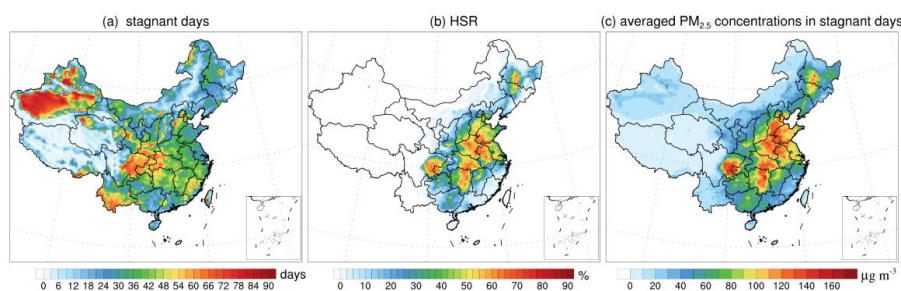
336

337 3.4 Pollution days in SWLY attributable to atmospheric stagnation

338 Stagnant meteorological conditions have been found to play an important role in
 339 promoting accumulation of $PM_{2.5}$ on severe pollution days in China (Wang et al., 2022;
 340 Wang et al., 2018a). Therefore, besides of the days categorized as seesaw pattern in
 341 wintertime during 2014-2019, we investigate the impact of atmospheric stagnation on
 342 $PM_{2.5}$ pollution in SWLY.



343 The annual mean of atmospheric stagnation days in 2014-2019 over eastern China
344 is shown in Fig. 5a. The Tarim Basin and Sichuan Basin exhibit the most frequent
345 stagnation occurrence exceeding 50%, which is attributable to the topography as well
346 as climate conditions featured by low wind speed (Huang et al., 2017; Wang et al.,
347 2022). While in SWLY (green square in Fig. 1a), the annual mean stagnation days
348 reaches 37 days. Furthermore, we evaluate the capability of stagnation days to modulate
349 $PM_{2.5}$ pollution and use the ratio of polluted days in stagnation days to the total number
350 of stagnation days (HSR, defined in Gao et al. (2020)). As shown in Fig. 5b, among all
351 the stagnation days, the pollution days in SWLY account for 60%, which can explain
352 35% of the total pollution days (Table S3), implying the importance of stagnant weather
353 on the accumulation of $PM_{2.5}$. Under the stagnant condition, the spatial distribution of
354 average $PM_{2.5}$ concentration (Fig. 5c) shows explicit spatial heterogeneity that high
355 $PM_{2.5}$ concentration is captured in SWLY ($120.5 \mu g m^{-3}$).



356

357 Figure 5. The annual total number of stagnant days(a), ratio of the pollution days to the
358 total number of stagnant days (HSR, b) and mean $PM_{2.5}$ concentrations during stagnant
359 days during winter 2014-2019.

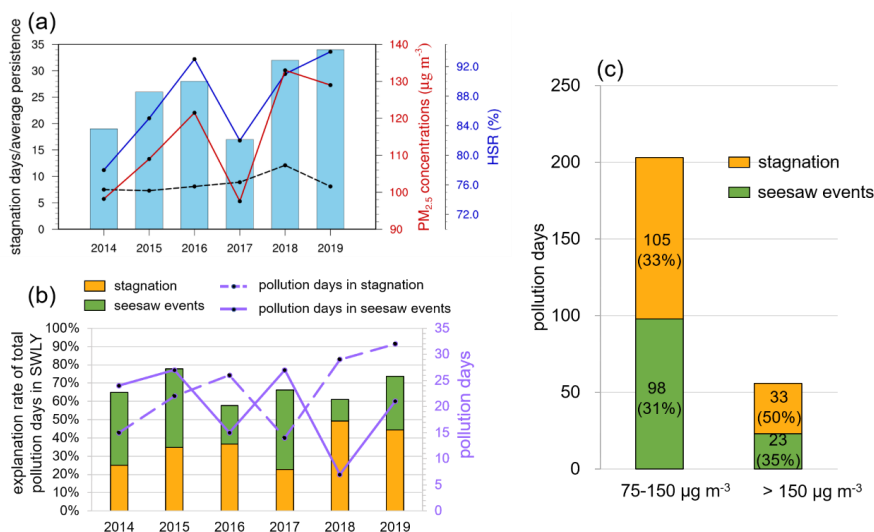
360

361 Furthermore, the interannual variability of winter total stagnation days composited
362 mean $PM_{2.5}$ concentrations during stagnation and HSR are displayed in Fig. 6a,
363 indicating consistently positive trends for the three metrics. The variability of HSR and
364 composited mean $PM_{2.5}$ concentrations are likely governed by the variability of
365 stagnation persistence (depicted as the black dotted line in Fig. 6a). When focusing
366 specifically on pollution days (defined as daily mean $PM_{2.5}$ concentration exceeding 75



367 $\mu\text{g m}^{-3}$) only during atmospheric stagnation, which is equivalent to the product of
 368 stagnation days and HSR, yielding on average of 23 days per winter and accounting for
 369 23%-49% (orange bars in Fig. 6b) of total pollution days during the winter of 2014-
 370 2019. Moreover, the total number of pollution days amounts to 387 (Table S3). The
 371 pollution days associated with seesaw events are laid out in green bars and account for
 372 a range of 12% to 44%, with highest proportion of 44% in 2017, following by 43% in
 373 2015 and 40% in 2014, tightly linked to the interannual variability of large-scale cold
 374 fronts activities (Zhang et al., 2019c). Overall, the stagnation of air conditions and
 375 transport account for 58%-78%, on average of 67%, of the pollution days in SWLY in
 376 winter 2014-2019.

377 The pollution days can be classified into moderate pollution days ($75 \mu\text{g m}^{-3} <$
 378 $\text{PM}_{2.5} \leq 150 \mu\text{g m}^{-3}$) and heavy pollution days ($150 \mu\text{g m}^{-3} < \text{PM}_{2.5}$). For moderate
 379 pollution days, comparable contribution from stagnation (33%) and seesaw events
 380 (31%) is achieved. The contribution to the heavy pollution is even higher, accounting
 381 for 85%, with 50% from stagnation and 35% from seesaw events.



382

383 Figure 6. (a) annual stagnation days in winter (blue bars), the average concentration of
 384 $\text{PM}_{2.5}$ during stagnation period (red line), HSR (the ratio of haze days during stagnation
 385 period to the total number of stagnation days; blue line) and the average persistence of



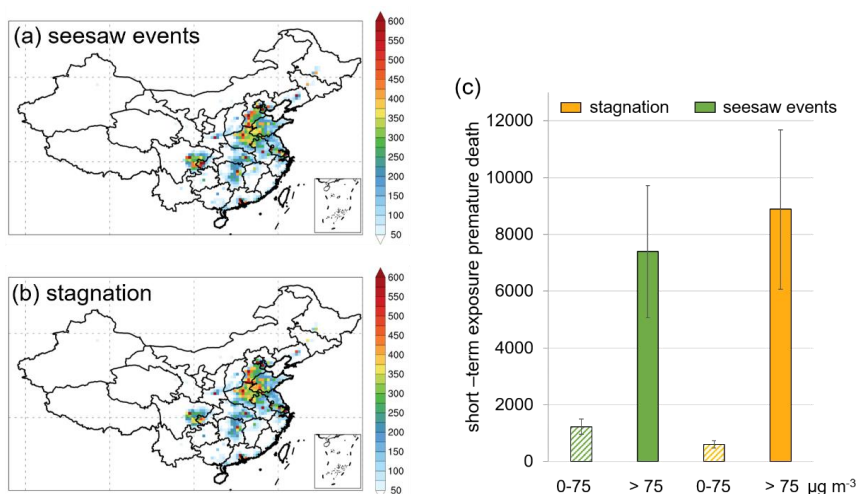
386 composite stagnation events in SWLY (black dotted line) in winter from 2014-2019. (b)
387 the annual explanation rate of stagnant air conditions and seesaw events on total
388 pollution days ($\text{PM}_{2.5}$ concentrations greater than $75 \mu\text{g m}^{-3}$) in SWLY. (c) the total
389 explanation rate of air stagnation and seesaw events on moderate pollution ($75\text{-}150 \mu\text{g}$
390 m^{-3}) and heavy pollution ($>150 \mu\text{g m}^{-3}$) days in SWLY.

391 **3.5 Premature deaths attributable to short-term $\text{PM}_{2.5}$ exposure over SWLY**

392 Considering the threat of exposure to $\text{PM}_{2.5}$ to public health, we have conducted
393 an assessment of premature deaths in SWLY due to short-term $\text{PM}_{2.5}$ exposure caused
394 by the seesaw events and stagnant meteorology in winter during 2014-2019.

395 There is a total of 26,241 (95% CI: 18,304-34,126) premature deaths resulting
396 from $\text{PM}_{2.5}$ exposure in SWLY in winter during 2014-2019. Specifically, during the
397 seesaw events as shown in Fig. 7a, focusing on the eastern China, the distribution of
398 premature deaths due to short-term $\text{PM}_{2.5}$ exposure mainly concentrate in southern NCP,
399 SWLY and YRD. For SWLY, the $\text{PM}_{2.5}$ exposure during the seesaw events accounts for
400 33% (8,634 (95% CI: 6,023-11,223)) of the total premature deaths, primarily due to the
401 exposure to pollution days (7,404 (95% CI: 5,060-9,727)) compared to clean days
402 (green bars in Fig. 7c). A comparable premature death is caused by stagnation (9,496
403 (95% CI: 6,552-12,413); Fig. 7b) in SWLY mainly attributable to $\text{PM}_{2.5}$ exposure in
404 pollution days (8,892 (95% CI: 6,078-11,678); orange bards in Fig. 7c). We also
405 calculate the total number of premature deaths in China during winter from 2014 to
406 2019 due to short-term exposure, which amount to 293,652 (95% CI: 229,711-357,318).
407 Notably, SWLY account for 9% of these premature deaths, despite its coverage
408 representing only 0.8% of the total land area.

409



410

411 Figure 7. (a) The spatial distribution of total premature deaths resulting from short-term
 412 PM_{2.5} exposure during the transport days (i.e., days with seesaw events); (b) Same as
 413 (a) but for the days with stagnation conditions in SWLY; (c) The premature deaths
 414 resulting from exposure to PM_{2.5} which concentrations is less than 75 µg m⁻³ and greater
 415 than 75 µg m⁻³ during transport and stagnant days in SWLY.

416

417 Conclusions

418 The SWLY region, located at the junction of the NCP and YRD, experiences a
 419 persistent and pronounced wintertime PM_{2.5} pollution situation from 2014 to 2019.
 420 Interestingly, despite comparable frequencies of pollution days between NCP and
 421 SWLY, the total number of pollution days in SWLY (57.1 days per year) is 14% higher
 422 than in NCP. This can be attributed to the amplified influence of seesaw transport effects
 423 between NCP and YRD on PM_{2.5} levels in SWLY.

424 When there is a transition in the geopotential height anomaly at 500 hPa,
 425 particularly when it changes from positive to negative in northern China (or vice versa),
 426 it leads to a shift in pollutant transport. The northwest wind activity facilitates the
 427 transport of pollutants from NCP to YRD, while the southeasterly wind favors pollutant
 428 transports from YRD to NCP, yielding high PM_{2.5} levels in SWLY. Moreover,
 429 atmospheric stagnation plays a crucial role in triggering PM_{2.5} accumulation in SWLY.
 430 For instance, during the winter period of 2014-2019, both the total number of stagnation
 431 days and mean PM_{2.5} concentration during stagnant periods show positive trends, likely



432 modulated by the persistence of stagnation. Overall, the combined influence of seesaw
433 events and stagnation account for approximately two thirds of the pollution days
434 observed in SWLY.

435 Considering the health effects during winters from 2014 to 2019 in SWLY, short-
436 term exposure to PM_{2.5} is found to result in additional 8,634 premature deaths (95% CI:
437 6,023-11,223) and 9,496 premature deaths (95% CI: 6,552-12,413) attributable to
438 seesaw events and stagnation, respectively. Despite the area of SWLY covers less than
439 1% in China, the total number of premature deaths in SWLY accounted for 9%. More
440 frequent atmospheric stagnation events are projected to occur in China under a warming
441 climate (Horton et al., 2014; Hu et al., 2022), highlighting the urgency of coordinated
442 cross-regional emissions reduction to achieve additional benefits in reducing PM_{2.5}
443 concentrations and the associated health effect in SWLY.

444

445 **Data availability**

446 The regional air quality simulations are available upon request to the corresponding
447 author.

448

449 **Author contributions**

450 Y.G. conceived the project, Y.F.F performed the analysis and drafted the manuscript,
451 and all authors contributed to the writing of the manuscript.

452

453 **Competing interests.** At least one of the (co-)authors is a member of the editorial board
454 of Atmospheric Chemistry and Physics.

455

456 **Acknowledgement**

457 This work was supported by the National Natural Science Foundation of China
458 (42122039) and Fundamental Research Funds for the Central Universities (202341001).
459 The simulations were conducted on the Center for High Performance Computing and
460 System Simulation, National Laboratory for Marine Science and Technology (Qingdao).



461

462 **References**

- 463 Appel, K.W., Bash, J.O., Fahey, K.M., Foley, K.M., Gilliam, R.C., Hogrefe, C., et al., 2021. The
464 Community Multiscale Air Quality (CMAQ) model versions 5.3 and 5.3.1: system updates and
465 evaluation. *Geoscientific Model Development*. 14, 2867-2897.
- 466 Appel, K.W., Gilliland, A.B., Sarwar, G., Gilliam, R.C., 2007. Evaluation of the Community Multiscale
467 Air Quality (CMAQ) model version 4.5: Sensitivities impacting model performance: Part I—
468 Ozone. *Atmospheric Environment*. 41, 9603-9615.
- 469 Berman, A., Adhikari, T., Mukhopadhyay, S., Baraki, A., Tessema, Z., 2020. Global burden of 369
470 diseases and injuries in 204 countries and territories, 1990–2019: a systematic analysis for the.
471 Donaldson, K., Li, X.Y., MacNee, W., 1998. Ultrafine (nanometre) particle mediated lung injury. *Journal*
472 *of Aerosol Science*. 29, 553-560.
- 473 Emery, C., Tai, E. Enhanced Meteorological Modeling and Performance Evaluation for Two Texas Ozone
474 Episodes, 2001.
- 475 Emmons, L.K., Walters, S., Hess, P.G., Lamarque, J.F., Pfister, G.G., Fillmore, D., et al., 2010.
476 Description and evaluation of the Model for Ozone and Related chemical Tracers, version 4
477 (MOZART-4). *Geoscientific Model Development*. 3, 43-67.
- 478 EPA, U. Guidance on the Use of Models and Other Analyses for Demonstrating Attainment of Air Quality
479 Goals for Ozone, PM_{2.5} and Regional Haze. Vol EPA -454/B-07-002, 2007.
- 480 Gao, Y., Zhang, L., Huang, A., Kou, W., Bo, X., Cai, B., et al., 2022. Unveiling the spatial and sectoral
481 characteristics of a high-resolution emission inventory of CO₂ and air pollutants in China.
482 *Science of The Total Environment*. 847, 157623.
- 483 Gao, Y., Zhang, L., Zhang, G., Yan, F.F., Zhang, S.Q., Sheng, L.F., et al., 2020. The climate impact on
484 atmospheric stagnation and capability of stagnation indices in elucidating the haze events over
485 North China Plain and Northeast China. *Chemosphere*. 258, 12.
- 486 Giglio, L., Randerson, J.T., van der Werf, G.R., 2013. Analysis of daily, monthly, and annual burned area
487 using the fourth-generation global fire emissions database (GFED4). *Journal of Geophysical*
488 *Research-Biogeosciences*. 118, 317-328.
- 489 Guenther, A.B., Jiang, X., Heald, C.L., Sakulyanontvittaya, T., Duhl, T., Emmons, L.K., et al., 2012. The
490 Model of Emissions of Gases and Aerosols from Nature version 2.1 (MEGAN2.1): an extended
491 and updated framework for modeling biogenic emissions. *Geoscientific Model Development*.
492 5, 1471-1492.
- 493 He, J., Gong, S., Zhou, C., Lu, S., Wu, L., Chen, Y., et al., 2018. Analyses of winter circulation types and
494 their impacts on haze pollution in Beijing. *Atmospheric Environment*. 192, 94-103.
- 495 Horton, D.E., Skinner, C.B., Singh, D., Diffenbaugh, N.S., 2014. Occurrence and persistence of future
496 atmospheric stagnation events. *Nature Climate Change*. 4, 698-703.
- 497 Hu, A., Xie, X., Gong, K., Hou, Y., Zhao, Z., Hu, J., 2022. Assessing the Impacts of Climate Change on
498 Meteorology and Air Stagnation in China Using a Dynamical Downscaling Method. *Frontiers*
499 *in Environmental Science*. 10.
- 500 Hua, W.L., Wu, B.Y., 2022. Atmospheric circulation anomaly over mid- and high-latitudes and its
501 association with severe persistent haze events in Beijing. *Atmospheric Research*. 277.
- 502 Huang, Q.Q., Cai, X.H., Song, Y., Zhu, T., 2017. Air stagnation in China (1985-2014): climatological
503 mean features and trends. *Atmospheric Chemistry and Physics*. 17, 7793-7805.



- 504 Huang, X., Ding, A.J., Wang, Z.L., Ding, K., Gao, J., Chai, F.H., et al., 2020. Amplified transboundary
505 transport of haze by aerosol-boundary layer interaction in China. *Nature Geoscience*. 13, 428-
506 +.
- 507 Jia, Z.X., Doherty, R.M., Ordonez, C., Li, C.F., Wild, O., Jain, S., et al., 2022. The impact of large-scale
508 circulation on daily fine particulate matter (PM_{2.5}) over major populated regions of China in
509 winter. *Atmospheric Chemistry and Physics*. 22, 6471-6487.
- 510 Jiang, Z., Jolleys, M.D., Fu, T.-M., Palmer, P.I., Ma, Y., Tian, H., et al., 2020. Spatiotemporal and
511 probability variations of surface PM_{2.5} over China between 2013 and 2019 and the associated
512 changes in health risks: An integrative observation and model analysis. *Science of The Total
513 Environment*. 723, 137896.
- 514 Kang, H.Q., Zhu, B., Gao, J.H., He, Y., Wang, H.L., Su, J.F., et al., 2019. Potential impacts of cold frontal
515 passage on air quality over the Yangtze River Delta, China. *Atmospheric Chemistry and Physics*.
516 19, 3673-3685.
- 517 Kang, H.Q., Zhu, B., Liu, X.H., Shi, S.S., Hou, X.W., Lu, W., et al., 2021. Three-Dimensional
518 Distribution of PM_{2.5} over the Yangtze River Delta as Cold Fronts Moving Through. *Journal
519 of Geophysical Research-Atmospheres*. 126, 11.
- 520 Li, J.D., Liao, H., Hu, J.L., Li, N., 2019a. Severe particulate pollution days in China during 2013-2018
521 and the associated typical weather patterns in Beijing-Tianjin-Hebei and the Yangtze River
522 Delta regions. *Environmental Pollution*. 248, 74-81.
- 523 Li, M., Liu, H., Geng, G.N., Hong, C.P., Liu, F., Song, Y., et al., 2017. Anthropogenic emission
524 inventories in China: a review. *National Science Review*. 4, 834-866.
- 525 Li, T.T., Guo, Y.M., Liu, Y., Wang, J.N., Wang, Q., Sun, Z.Y., et al., 2019b. Estimating mortality burden
526 attributable to short-term PM_{2.5} exposure: A national observational study in China.
527 *Environment International*. 125, 245-251.
- 528 Liu, C., Chen, R., Sera, F., Vicedo-Cabrera, A.M., Guo, Y., Tong, S., et al., 2019a. Ambient Particulate
529 Air Pollution and Daily Mortality in 652 Cities. *New England Journal of Medicine*. 381, 705-
530 715.
- 531 Liu, H., Fu, M.L., Jin, X.X., Shang, Y., Shindell, D., Faluvegi, G., et al., 2016. Health and climate impacts
532 of ocean-going vessels in East Asia. *Nature Climate Change*. 6, 1037-+.
- 533 Liu, H., Meng, Z.H., Lv, Z.F., Wang, X.T., Deng, F.Y., Liu, Y., et al., 2019b. Emissions and health impacts
534 from global shipping embodied in US-China bilateral trade. *Nature Sustainability*. 2, 1027-1033.
- 535 Liu, J., Yin, H., Tang, X., Zhu, T., Zhang, Q., Liu, Z., et al., 2021. Transition in air pollution, disease
536 burden and health cost in China: A comparative study of long-term and short-term exposure.
537 *Environmental Pollution*. 277.
- 538 Luecken, D.J., Yarwood, G., Hutzell, W.T., 2019. Multipollutant modeling of ozone, reactive nitrogen
539 and HAPs across the continental US with CMAQ-CB6. *Atmospheric Environment*. 201, 62-72.
- 540 Ma, M.C., Gao, Y., Wang, Y.H., Zhang, S.Q., Leung, L.R., Liu, C., et al., 2019. Substantial ozone
541 enhancement over the North China Plain from increased biogenic emissions due to heat waves
542 and land cover in summer 2017. *Atmospheric Chemistry and Physics*. 19, 12195-12207.
- 543 Ma, Q.X., Wu, Y.F., Zhang, D.Z., Wang, X.J., Xia, Y.J., Liu, X.Y., et al., 2017. Roles of regional transport
544 and heterogeneous reactions in the PM_{2.5} increase during winter haze episodes in Beijing.
545 *Science of the Total Environment*. 599, 246-253.
- 546 MEEPRC. Technical regulation on ambient air quality index (on trial): HJ 633. 2022, 2012.
- 547 Pui, D.Y.H., Chen, S.C., Zuo, Z.L., 2014. PM_{2.5} in China: Measurements, sources, visibility and health



- 548 effects, and mitigation. *Particuology*. 13, 1-26.
- 549 Pye, H.O.T., Murphy, B.N., Xu, L., Ng, N.L., Carlton, A.G., Guo, H.Y., et al., 2017. On the implications
550 of aerosol liquid water and phase separation for organic aerosol mass. *Atmospheric Chemistry
551 and Physics*. 17, 343-369.
- 552 Saha, S., Moorthi, S., Wu, X.R., Wang, J., Nadiga, S., Tripp, P., et al., 2014. The NCEP Climate Forecast
553 System Version 2. *Journal of Climate*. 27, 2185-2208.
- 554 Sun, Y., Zhang, Y., Chen, C., Sun, Q., Wang, Y., Du, H., et al., 2022. Impact of Heavy PM(2.5) Pollution
555 Events on Mortality in 250 Chinese Counties. *Environmental Science & Technology*. 56, 8299-
556 8307.
- 557 Van der Werf, G.R., Randerson, J.T., Giglio, L., van Leeuwen, T.T., Chen, Y., Rogers, B.M., et al., 2017.
558 Global fire emissions estimates during 1997-2016. *Earth System Science Data*. 9, 697-720.
- 559 Wang, J., Liu, Y., Ding, Y., Wu, P., Zhu, Z., Xu, Y., et al., 2020. Impacts of climate anomalies on the
560 interannual and interdecadal variability of autumn and winter haze in North China: A review.
561 *International Journal of Climatology*. 40, 4309-4325.
- 562 Wang, L.H., Newchurch, M.J., Biazar, A., Liu, X., Kuang, S., Khan, M., et al., 2011. Evaluating
563 AURA/OMI ozone profiles using ozonesonde data and EPA surface measurements for August
564 2006. *Atmospheric Environment*. 45, 5523-5530.
- 565 Wang, L.L., Li, M.G., Wang, Q.L., Li, Y.Y., Xin, J.Y., Tang, X., et al., 2022. Air stagnation in China:
566 Spatiotemporal variability and differing impact on PM2.5 and O₃ during 2013-2018. *Science
567 of the Total Environment*. 819.
- 568 Wang, X.Y., Dickinson, R.E., Su, L.Y., Zhou, C.L.E., Wang, K.C., 2018a. PM2.5 POLLUTION IN
569 CHINA AND HOW IT HAS BEEN EXACERBATED BY TERRAIN AND
570 METEOROLOGICAL CONDITIONS. *Bulletin of the American Meteorological Society*. 99,
571 105-120.
- 572 Wang, X.Y., Dickinson, R.E., Su, L.Y., Zhou, C.L.E., Wang, K.C., 2018b. PM2.5 pollution in China and
573 how it has been exacerbated by terrain and meteorological conditons. *Bulletin of the American
574 Meteorological Society*. 99, 105-120.
- 575 Wang, Y.S., Yao, L., Wang, L.L., Liu, Z.R., Ji, D.S., Tang, G.Q., et al., 2014. Mechanism for the formation
576 of the January 2013 heavy haze pollution episode over central and eastern China. *Science China-
577 Earth Sciences*. 57, 14-25.
- 578 Wu, X.G., Ding, Y.Y., Zhou, S.B., Tan, Y., 2018. Temporal characteristic and source analysis of PM2.5
579 in the most polluted city agglomeration of China. *Atmospheric Pollution Research*. 9, 1221-
580 1230.
- 581 Xie, Y., Dai, H.C., Dong, H.J., Hanaoka, T., Masui, T., 2016. Economic Impacts from PM2.5 Pollution-
582 Related Health Effects in China: A Provincial-Level Analysis. *Environmental Science &
583 Technology*. 50, 4836-4843.
- 584 Xing, Y.F., Xu, Y.H., Shi, M.H., Lian, Y.X., 2016. The impact of PM2.5 on the human respiratory system.
585 *Journal of Thoracic Disease*. 8, E69-E74.
- 586 Yang, Y., Luo, L.W., Song, C., Yin, H., Yang, J.T., 2018. Spatiotemporal Assessment of PM2.5-Related
587 Economic Losses from Health Impacts during 2014-2016 in China. *International Journal of
588 Environmental Research and Public Health*. 15.
- 589 Zeng, X.R., Gao, Y., Wang, Y.H., Ma, M.C., Zhang, J.X., Sheng, L.F., 2022. Characterizing the distinct
590 modulation of future emissions on summer ozone concentrations between urban and rural areas
591 over China. *Science of the Total Environment*. 820, 11.



- 592 Zhang, G., Gao, Y., Cai, W., Leung, L.R., Wang, S., Zhao, B., et al., 2019a. Seesaw haze pollution in
593 North China modulated by the sub-seasonal variability of atmospheric circulation. *Atmos.*
594 *Chem. Phys.* 19, 565-576.
- 595 Zhang, J., Yuan, Q., Liu, L., Wang, Y.Y., Zhang, Y.X., Xu, L., et al., 2021a. Trans-Regional Transport of
596 Haze Particles From the North China Plain to Yangtze River Delta During Winter. *Journal of*
597 *Geophysical Research-Atmospheres.* 126.
- 598 Zhang, Q., Quan, J.N., Tie, X.X., Li, X., Liu, Q., Gao, Y., et al., 2015. Effects of meteorology and
599 secondary particle formation on visibility during heavy haze events in Beijing, China. *Science*
600 *of the Total Environment.* 502, 578-584.
- 601 Zhang, Q., Zheng, Y.X., Tong, D., Shao, M., Wang, S.X., Zhang, Y.H., et al., 2019b. Drivers of improved
602 PM_{2.5} air quality in China from 2013 to 2017. *Proceedings of the National Academy of*
603 *Sciences of the United States of America.* 116, 24463-24469.
- 604 Zhang, S., Zeng, G., Wang, T., Yang, X., Iyakaremye, V., 2022. Three dominant synoptic atmospheric
605 circulation patterns influencing severe winter haze in eastern China. *Atmos. Chem. Phys.* 22,
606 16017-16030.
- 607 Zhang, W., Hai, S., Zhao, Y., Sheng, L., Zhou, Y., Wang, W., et al., 2021b. Numerical modeling of
608 regional transport of PM_{2.5} during a severe pollution event in the Beijing–Tianjin–Hebei region
609 in November 2015. *Atmospheric Environment.* 254, 118393.
- 610 Zhang, X., Xu, X., Ding, Y., Liu, Y., Zhang, H., Wang, Y., et al., 2019c. The impact of meteorological
611 changes from 2013 to 2017 on PM_{2.5} mass reduction in key regions in China. *Science China*
612 *Earth Sciences.* 62, 1885-1902.
- 613 Zheng, B., Tong, D., Li, M., Liu, F., Hong, C.P., Geng, G.N., et al., 2018. Trends in China's anthropogenic
614 emissions since 2010 as the consequence of clean air actions. *Atmospheric Chemistry and*
615 *Physics.* 18, 14095-14111.
- 616 Zhong, W., Yin, Z., Wang, H., 2019. The relationship between anticyclonic anomalies in northeastern
617 Asia and severe haze in the Beijing–Tianjin–Hebei region. *Atmos. Chem. Phys.* 19, 5941-5957.
- 618